Eurasian Chem.-Technol. J. 27 (2026) 25–43
The journal of the Institute of Combustion Problems https://ect-journal.kz

https://doi.org/10.18321/ectj1681

Implementation and Validation of a REDIM-Based CFD Solver for Combustion Applications

Ningyi Li[1*], Thorsten Zirwes[2], Ulrich Maas[1]

[1]Institute of Technical Thermodynamics, Karlsruhe Institute of Technology, Engelbert-Arndold-Strasse 4, Karlsruhe, 76131, Germany
[2]Institute for Reactive Flows, University of Stuttgart, Pfaffenwaldring 31, Stuttgart, 70569, Germany

Article info

Received:
16 October 2025

Received in revised form:
26 December 2025

Accepted:
18 February 2026

Keywords:
Reaction-diffusion manifolds (REDIM);
Laminar flames;
Direct numerical simulation (DNS);
Reduced chemistry;
Flame extinction

Abstract

The complexity of the combustion process makes the computational time using a detailed mechanism unacceptable, therefore, it is necessary to simplify the mechanism. The reaction-diffusion manifolds (REDIM) method is a reduction model that takes the coupling of molecular diffusion and chemical reactions into account to reduce computing times, and can be utilized in different types of combustion simulations. In this work, the REDIM method is implemented into a new OpenFOAM-based CFD solver. The use of both generalized and physical coordinates to represent the manifold is analyzed for freely propagating laminar flames. The REDIM-based solver is then used to calculate 2D laminar counterflow flames. Different detailed mechanisms, progress variables and inlet velocities are applied to calculate the 2D counterflow flames and to evaluate the performance of REDIM at steady and extinction conditions. It is shown that the results computed by the REDIM method have good agreement with the results obtained by detailed simulations. Furthermore, the REDIM method offers a significant reduction in computational cost in the newly developed solver.

1. Introduction

Accurate numerical simulations of combustion have generated continuous interest over the past few decades. However, the time scales of chemical processes typically span several orders of magnitude, with chemical reactions in combustion processes usually covering a range from 10^{-10} to 10^{0} s [1]. Consequently, the implementation of detailed chemical kinetics in simulations of practical combustion devices (e.g. engines, gas turbines, and industrial furnaces) is related a large stiffness of the governing equation system and very high computational costs. Given the limitations imposed by current computing power, the development of efficient techniques for reduced kinetics holds significant importance.

Based on the fact that the chemical time scale and length scale of most flames are very small, there are two popular routes in numerical combustion to reduce the number of governing equations: chemical reduction techniques and flamelet models [2]. Chemical reduction techniques assume that the fast time scales of chemical reactions are typically responsible for the equilibration processes, which include quasi-steady state assumption (QSSA) [3], partial-equilibrium approximation (PEA) [4], intrinsic low-dimensional manifolds (ILDM) [5], computational singular perturbation (CSP) [6], etc. To improve the performance of ILDM and CSP in the low-temperature domain, different methods have been proposed, e.g. flame prolongation of ILDM (FPI) [7] and extended ILDM [8]. With these methods, significant improvement in the performance of ILDM and CSP in the low-temperature region can be achieved, with a notable reduction in computational cost.

*Corresponding author.
E-mail address: ningyi.li@partner.kit.edu

In contrast to other reduction approaches, flamelet generated manifold (FGM) [9] and reaction-diffusion manifolds (REDIM) apply the concept of invariant manifolds taking into account the coupling of molecular transport and chemical reaction processes [10]. The REDIM serves as an approach to reduce complex kinetics to low dimensional manifolds, which can be applied to various combustion scenarios. The REDIM method offers two significant advantages: It requires little knowledge of the combustion regime when generating the REDIM, and encompasses both steady and transient processes (e.g. ignition and extinction). In prior research [11–17], the REDIM method was used to calculate different flame configurations, including premixed flames, steady and transient counterflow flames, and turbulent flames. These results obtained with the REDIM demonstrated very good concordance with detailed simulations and experimental measurements.

In the OpenFOAM framework [18] with the REDIM method, Luo et al. [19, 20] calculated examples of wall-flame interactions implemented in generalized coordinates, and Shrotriya et al. [21, 22] simulated partially-premixed flames using physical coordinates. The main focus of this paper is to build a REDIM-based CFD solver using generalized/physical coordinates in OpenFOAM and validate its performance in combustion applications [23]. In order to achieve the purpose, this work needs to address the following questions:

- What are suitable benchmark cases?
- What impact does REDIM–using either generalized and physical coordinates–have on the accuracy of the solution?
- How does REDIM perform with different mesh sizes, progress variables, reaction mechanisms and flow velocities?
- Can the REDIM predict extinction states not explicitly given during manifold generation?

Freely propagating flames and counterflow flames are widely used in numerical combustion to investigate the precision and accuracy of models [1, 24]. In this work, we use these two types of flames to verify the performance of the REDIM model. To generate validation data, the OpenFOAM-based EBIdnsFoam solver was used [25, 26], which computes reaction rates with the detailed finite-rate chemistry model and uses detailed diffusion models for each species as well.

The paper is organized as follows. Section 2 introduces the mathematical basics of the system describing combustion with detailed chemical mechanisms, as used in the EBIdnsFoam solver. The main focus of section 3 presents the mathematical background of the REDIM reduced chemistry, an example of constructing a REDIM table for a diffusion methane/air flame, and the implementation procedure of the REDIM method in physical and generalized coordinates. The REDIM method in generalized and physical coordinates is investigated by simulating an adiabatic 1D premixed methane/air free flame in section 4. The application of the REDIM method to 2D counterflow flames is discussed in section 5. Results with three different mesh resolutions are calculated to study the mesh dependence with finite rate chemistry and the corresponding REDIM reduced method. Two different linear combinations of parametrization are selected to examine the independence of the REDIM reduced model with respect to the progress variable. The profiles of temperature and mass fractions computed by the REDIM reduced chemistry in the flame structures are compared to the detailed solutions with different mechanisms, which verify the performance o REDIM with different detailed mechanisms. The peak temperature, mass fractions and state space during extinction are used to validate the behaviour of REDIM at steady and transient extinction conditions. Finally, conclusion are drawn in section 6.

2. Detailed governing equations

The combustion process based on detailed chemical mechanisms is described mathematically by the following governing equations (assuming a Newtonian fluid) [24]

- Continuity equation:

$$\frac{\partial \rho}{\partial t} + \nabla \cdot \left(\rho U\right) = 0, \tag{1}$$

where ρ denotes the density, t is the time and U is the velocity vector.

- Species mass fraction equation:

$$\frac{\partial \left(\rho Y_k\right)}{\partial t} + \nabla \cdot \left(\rho Y_k \left(U + U_c\right)\right) + \nabla \cdot j_k = \dot{\omega}_k, \quad k = 1, \ldots, n_s - 1 \tag{2}$$

where Y_k is the mass fraction of species k, U_c represents the correction velocity [24], $\dot{\omega}_k$ is the reaction rate of species k, and j_k denotes the diffusive mass flux density of species k, with n_s the number of species in the reacting system.

• Momentum equation:

$$\frac{\partial(\rho U)}{\partial t} = -\nabla\cdot(\rho U\otimes U)+\nabla\cdot\left[\mu\left(\nabla\otimes U+(\nabla\otimes U)^T-\frac{2}{3}(\nabla\cdot U)I\right)\right]-\nabla p+\rho g, \tag{3}$$

where the symbol $U\otimes U$ denotes the outer (dyadic) product of two velocity vectors, μ is the dynamic viscosity, I denotes the identity matrix, ∇p is the gradient of the pressure.

• Energy equation:

$$\frac{\partial(\rho h_s)}{\partial t}+\nabla\cdot(\rho U h_s) = -\frac{\partial(\rho K)}{\partial t}-\nabla\cdot(\rho U K)-\nabla\cdot q+\dot{\omega}_T+\frac{\partial p}{\partial t}+\nabla\cdot q_{\text{rad}}, \tag{4}$$

where h_s is the sensible enthalpy, $K=\frac{1}{2}|U|^2$ denotes the specific kinetic energy, q the heat flux vector, $\dot{\omega}_T$ is the heat release rate and the term q_{rad} is the radiative heat flux. The temperature is calculated from the sensible enthalpy via the heat capacity using Newton's method.

• Equation of state:

$$\rho=\frac{p\overline{M}}{RT}, \tag{5}$$

where R is the universal gas constant, $\overline{\text{M}}$ denotes the mean molar weight and T is the temperature.

In order to simulate the combustion process based on detailed mechanisms, we notice that the system of equations consisting of Eqs. (1)–(5) and (n_s–1) species equations is solved. The remaining species mass fraction is calculated $Y_s=1-\sum_{k=1}^{S-1}Y_k$ by to ensure mass conservation. By employing the Hirschfelder and Curtiss approximation, the Maxwell-Stefan equations can be simplified, resulting in a closed expression for the species diffusion flux density j_k [27]

$$j_k=-\rho D_k\nabla Y_k, \tag{6}$$

where D_k is the diffusion coefficient of species k into the rest of the mixture. If the assumption of unity Lewis number (Le_k = 1) is used, the diffusion coefficient D_k can be written as

$$D_k=\frac{\lambda}{\rho C_p}, \tag{7}$$

where λ denotes the thermal conductivity and C_p is the heat capacity at constant pressure.

An optically thin radiation model with three radiating species (H_2O, CO, CO_2) is taken into account [28, 29]. Based on the optically thin assumption, the radiative heat loss term is defined as [30]

$$\nabla\cdot q_{\text{rad}}=4\sigma\left(T^4-T_b^4\right)\sum_i\left(p_i a_{pi}\right), \tag{8}$$

where σ is the Stefan-Boltzmann constant, T_b denotes the environment temperature, p_i represents the partial pressure of species i in atmospheres and a_{pi} is the Planck mean absorption coefficient of species i.

The above set of governing equations is implemented into the DNS solver EBIdnsFoam [25, 26], which couples OpenFOAM [18] and Cantera [31]. The OpenFOAM part in the solver is used to solve the governing equations (i.e. total mass, momentum, energy and species conservation equations) and supplies the results of pressure, temperature and species mass fractions to Cantera. The Cantera part is used to compute detailed transport properties (molecular viscosity, thermal conductivity, species diffusion coefficients) and reaction rates. The EBIdnsFoam solver is applied to an axisymmetric laminar coflow diffusion flame, which will be presented in the supplementary material.

3. Reaction-Diffusion Manifolds (REDIM)

3.1. The REDIM method

The REDIM model (details see Ref. [10]) can be described by the detailed evolution equation of a typical reacting flow with the (n = n_s+2)-dimensional state vector $\Psi=\left(h,p,\phi_1,...,\phi_{n_s}\right)^T$, which is written as

$$\frac{\partial\Psi}{\partial t}=F(\Psi)-U\cdot\nabla\Psi-\frac{1}{\rho}\nabla\cdot(D\cdot\nabla\Psi)\equiv\Phi(\Psi), \tag{9}$$

where h is the specific enthalpy, the ratio $\phi_k=\frac{Y_k}{M_k}$ denotes the specific mole number with mass fraction Y_k and corresponding species molar masses M_k, D represents the ($n\times n$)-dimensional diffusion matrix given via [1]. $F(\Psi)$ is the n-dimensional vector (F_p, F_h, $\dot{r}_1$, $\dot{r}_{n_s}$) that accounts for the chemical source terms, $\dot{\omega}_k,\dot{r}_{n_k}=\frac{\dot{\omega}_k}{M_k}$, F_p = 0 for an isobaric system, and in the cases considering thermal radiation, $F_h\neq 0$, Eq. (8) is used to calculate the radiative source term, which can be used in combustion systems where thermal

radiation is not negligible [32]. $\Phi(\Psi)$ is the vector valued function of the rates of change of the variables Ψ. As has been shown by correlation analysis of DNS data [33], the chemical states are in the vicinity of low-dimensional manifolds. The REDIM method identifies these m_s-dimensional manifolds [10] as

$$M = \left\{\Psi : \Psi = \Psi(\theta), \Psi : R^{m_s} \to R^n\right\}, \quad (10)$$

where $\Psi(\theta)$ is an explicit function parameterized by the variable θ (an m_s-dimensional vector of local coordinates) and M is the invariant m_s-dimensional system manifold, which can be used to describe the system solution of state space by m_s parameters instead of using n parameters ($m_s \ll n$).

According to the core concept of manifold dimension reduction, the problem of model reduction is transformed into the task of identifying and describing manifolds with the required properties [12]. For the PDE formed by Eq. (9), its invariant manifold must satisfy the condition

$$\left(I - \Psi_\theta \Psi_\theta^+\right) \cdot \Phi(\Psi) = 0, \quad (11)$$

where Ψ_θ is the matrix of partial derivatives of Ψ with respect to θ, I is the ($n \times n$)-dimensional identity matrix and Ψ_θ^+ is an ($m_s \times n$)-dimensional pseudo-inverse matrix of Ψ_θ (see [13] for possible definitions), which fulfills the condition

$$\Psi_\theta^+ \Psi_\theta = I_{m_s \times m_s}. \quad (12)$$

Note that for simplicity we assume equal diffusivities, that is, $D = d \cdot I$. However, the REDIM method has already been validated to correctly deal with effects of detailed molecular transport in syngas/air combustion systems where non-equal diffusivity plays an important role [34]. The convection term vanishes after projecting onto its normal component with the projection operator $I - \Psi_\theta \Psi_\theta^+$ due to $\Psi_\theta^+ \Psi_\theta = I$. Thus, the evolution equation for the invariant manifold can be written in a simplified form

$$\frac{\partial \Psi(\theta)}{\partial t} = \left(I - \Psi_\theta(\theta)\Psi_\theta^+(\theta)\right) \cdot \left(F(\Psi(\theta)) - \frac{1}{\rho}\left[\left(d\Psi_\theta \cdot \chi(\theta)\right)_\theta \cdot \chi(\theta)\right]\right), \quad (13)$$

where $\chi(\theta) = \text{grad}(\theta)$ is the gradient estimate of the manifold. With given initial conditions, boundary conditions and the gradient estimates, the REDIM is constructed in terms of Eq. (13). The generation procedure of REDIM has been implemented in the INSFLA and HOMREA codes [35], the details of which are found in [10, 13, 14].

Once the invariant manifold is generated, the n-dimensional state vector Ψ can be accessed as a function of m_s-dimensional parametrization vector θ, i.e. a back-transformation, which can be used to recover the species and temperature profiles [36]. In order to realize the transformation, Eq. (13) can be written in the following formulation by using the chain rule and multiplying both sides with the pseudo-inverse Ψ_θ^+

$$\frac{\partial \theta}{\partial t} = \Psi_\theta^+ \cdot F(\Psi(\theta)) - U \cdot \nabla\theta - \frac{1}{\rho}\Psi_\theta^+ \cdot \nabla \cdot \left(D\Psi_\theta \cdot \nabla\theta\right). \quad (14)$$

Finally, we can summarize the application procedure of the REDIM method in the following steps [10]:

- specify the initial condition, choose the suitable parametrization vector θ, and define the boundary condition for Eq. (13);
- supply the gradient estimate $\chi(\theta)$ as a function of the parameter θ for the evaluation equation;
- integrate Eq. (13) in time $t \to \infty$ until a stationary solution $\Psi(\theta)$ is obtained;
- store the data of θ, $\Psi(\theta)$, Ψ_θ, Ψ^+, $D\Psi_\theta$ and $\Psi^+_\theta F$, so that it can be used in Eq. (14).

As shown in [37], the evolution equation is invariant with respect to the reduced coordinate θ. In other words, the generation of the REDIM reduced chemistry is independent of the choice of θ. In order to verify this, results computed by the REDIM method with two different progress variables are compared in section 5.4. In the previous work, the specific mole number ϕ_{N_2} is usually selected as the first progress variable due to its monotonicity, which can be used to describe the mixing process. The choice of the second progress variable is arbitrary, as long as it can guarantee a one-to-one mapping (no folding part) of REDIM. Figure 1 shows the complete flow chart for the implementation procedure of the REDIM method. The terms $\Psi(\theta)$, Ψ_θ, Ψ^+_θ, $D\Psi_\theta$ and $\Psi_\theta^+ F$ are computed as functions of the local coordinates θ in a modified and extended version of HOMREA [35].

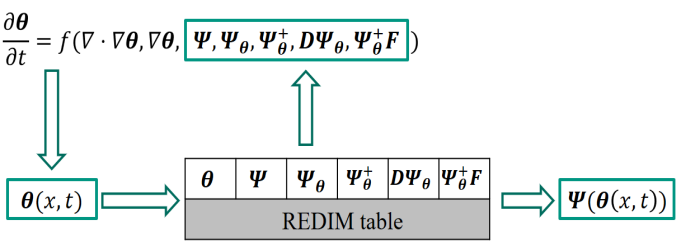

Fig. 1. Flow chart for the implementation procedure of REDIM [12, 13].

According to the above description of the implementation of REDIM, thee are only (3 + m_s) equations solved in the REDIM approach, namely Eq. (1), Eq. (3), Eq. (5), and m_s θ-equations (16). If m_s = 2, that is, $\theta = (\theta_1, \theta_2)^T$, then there are 2 θ-equations solved in the REDIMFoam solver.

3.2. Construction of REDIM for a counterflow methane/air flame

This section will provide a detailed description on how to create REDIM tables. To illustrate the process, we will use a typical example of a 1D laminar counterflow methane/air flame. A stream of methane mixed with air is injected from the left boundary while a stream of air is injected from the right boundary. The boundary conditions used to calculate the counterflow flame are listed in Table 1.

Table 1. Boundary conditions for the 1D counterflow flame

	T	*p*	Composition in volume percent
Left boundary	293 K	1 bar	25% CH_4 + 75% air
Right boundary	293 K	1 bar	21% O_2 + 79% N_2

In order to generate the REDIM tables, firstly we need to compute detailed solutions of different flame scenarios following the suggestions in Ref. [11]. These flame scenarios are a set of 1D counterflow flames with different strain rates in this example, which include reactive solutions and simple diffusion solutions. Schießl et al. [38] compared the REDIMs generated by the one- or multi-dimensional gradient estimates from DNS data and proved that gradient estimates have minor influence for the REDIMs in counterflow flames. Therefore, the REDIM obtained from the gradient estimate computed by 1D counterflow flames can accurately describe simulations with multi-dimensional transport. As mentioned above, the REDIM table is obtained by solving Eq. (13). To solve the equation, one must specify the initial condition, the boundary conditions and the gradient estimate.

The initial condition has been taken from stationary solutions of 1D counterflow flames. These stationary solutions are calculated by the in-house program INSFLA [35]. The strain rate α is an important quantity used to characterize 1D counterflow flames, which is defined and computed in Ref. [39]

$$a = \sqrt{-\frac{J}{\rho_{ub}}}, \tag{15}$$

where J denotes the tangential pressure gradient, and ρ_{ub} is the density of the unburnt fuel mixture.

Figure 2a shows the boundary conditions and the initial conditions taken from a collection of counterflow flames with different strain rates computed with the GRI3.0 mechanism. The upper boundary is a stationary solution with low strain rate of 80 s^{-1}. The pure mixing line is defined by the unburnt mixtures, that is, inert counterflow diffusion solution, which defines the lower boundary of the application range of REDIM. All possible flame scenarios in this work, consisting of both stable and unstable (extinction) flame regime, are between the upper and lower boundaries [14]. The boundaries of the manifold are specified as Dirichlet boundary conditions from the detailed flame calculation. Stationary solutions with different strain rates (α = 100, 120, 140, 160, 180, 200, 300 s^{-1}) are selected in this work. Any other states between two flamelets (represented by 3 black lines in Fig. 2 as an example) can be computed by a simple linear interpolation (red mesh), which is shown in Fig. 2b. Figure 2a is the projection of Fig. 2b on the specific mole number N_2 and CO_2 plane (the red mesh is not shown). The selection of initial solutions is arbitrary in theory, however, a reasonable initial guess can accelerate the convergence of Eq. (13). In order to highlight this point, we used a different initial guess to generate the REDIMs, that is, one REDIM (red mesh in Fig. 4) is generated by the flamelets (α = 80, 100, 120, 140, 160, 180, 200, 300 s^{-1} and mixing line), and the second REDIM (blue mesh in Fig. 4) is generated by only two flamelets (α = 80 s^{-1} and mixing line). Comparing the two REDIM manifolds, one can see that there are only slight differences between the final manifolds, however the convergence time in the REDIM with two flamelets is approximately 3 times that of the REDIM with the better initial guess. The REDIM method can also describe the extinction process very well, without providing any flamets in the extinction regime (for details see section 5.6.2).

Figure 3 shows that the gradient estimates for grad (N_2) and grad (CO_2) by (ϕ_{N_2}, ϕ_{CO_2}) used for the 2D REDIM are calculated by the 1D counterflow flamelets obtained with the GRI3.0 mechanism. Figure 4 shows examples of composition space of the 2D REDIM reduced chemistry in (ϕ_{N_2}, ϕ_{CO_2}) projection (the GRI3.0 mechanism is used in the example).

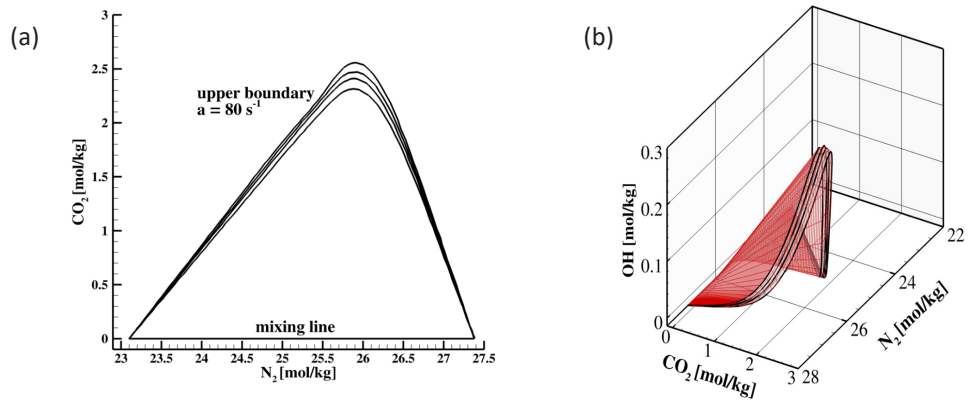

Fig. 2. Initial condition computed by the GRI3.0 mechanism for the construction of REDIM, flamelets at strain rate α = 80 s^{-1}, 140 s^{-1}, 200 s^{-1}, 300 s^{-1} and mixing line (a), linear interpolation between flamelets (b).

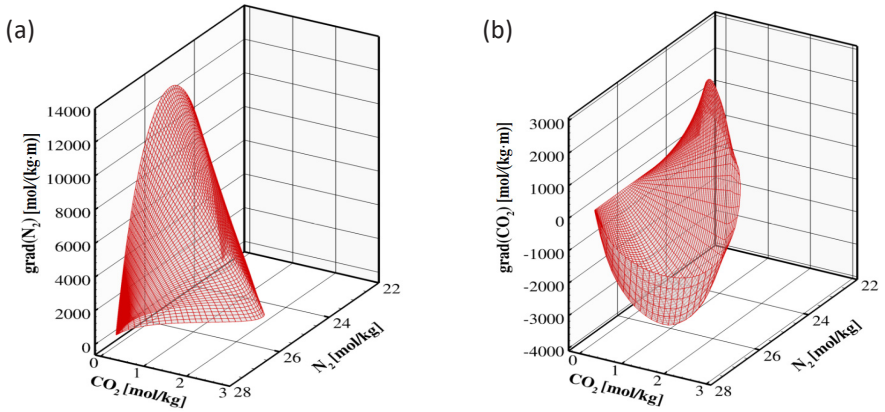

Fig. 3. Gradient estimate computed from 1D counterflow flamelets with the GRI3.0 mechanism for the construction of REDIM, grad (N_2) by (ϕ_{N_2}, ϕ_{CO_2}) (a), grad (CO_2) by (ϕ_{N_2}, ϕ_{CO_2}) (b).

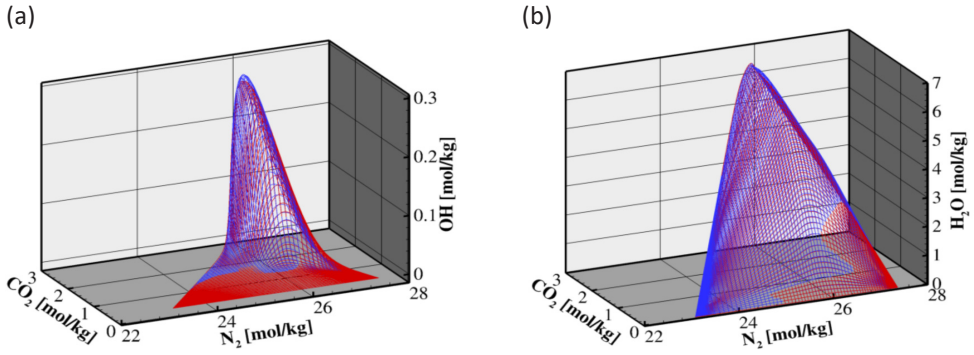

Fig. 4. Composition space of the 2D REDIM reduced chemistry in (ϕ_{N_2}, ϕ_{CO_2}) projection, OH (a) and H_2O (b).

3.3. REDIMFoam based on generalized coordinates

The system of governing equations used in the newly developed OpenFOAM-based REDIMFoam solver can be written as

- Continuity equation, same as Eq. (1)
- Reduced model equations for m_s-dimensional parametrization vector θ derived by combining Eq. (14) with the continuity equation:

$$\frac{\partial(\rho\theta)}{\partial t}+\nabla\cdot(\rho U\cdot\theta)+\Psi_\theta^+\cdot\nabla\cdot(D\Psi_\theta\cdot\nabla\theta)=\rho\Psi_\theta^+\cdot F(\Psi(\theta)). \quad (16)$$

- Momentum equation, same as Eq. (3)
- Equation of state, same as Eq. (5)

The numerical solution of REDIM generates an m_s-dimensional manifold on a mesh in the different coordinate directions and the evolution Eq. (13) is solved on the nodes of the mesh cell by cell [40]. The m_s-dimensional manifold is described by the grid indices (see Fig. 5), which are called generalized coordinates θ [36]. The generalized coordinates guarantee uniqueness and correspond to the reaction progress on the simplified manifold [36]. Furthermore, the generalized coordinates can also improve

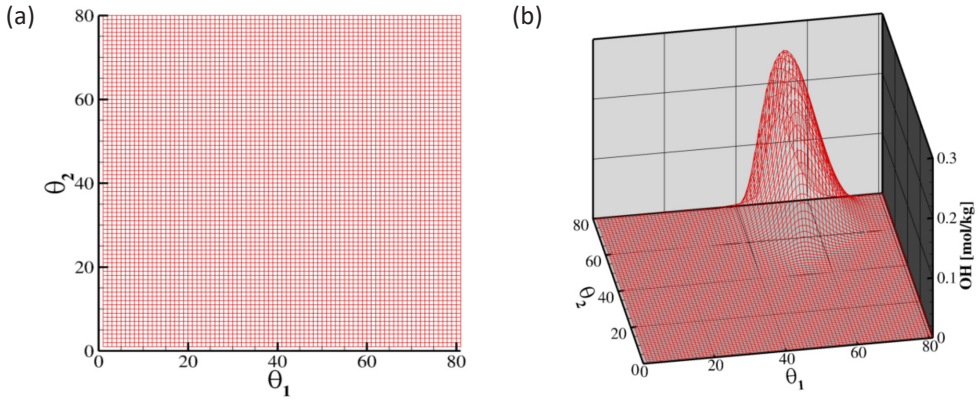

Fig. 5. Grid indices of a 2D REDIM table based on generalized coordinates, 2D projection of manifold in the generalized coordinates θ (a), 3D projection of OH profile (b).

the efficiency of interpolation during the implementation of REDIM, since the structure of the grid is locally orthogonal and equidistant everywhere.

As discussed before, the REDIM table has been generated in a pre-processing stage, and the terms $\Psi(\theta)$, Ψ_θ, Ψ_θ^+, $D\Psi_\theta$ and Ψ_θ^+F are computed at each mesh point and stored in the table beforehand. The next stage is the implementation of the system of governing equations in OpenFOAM. The REDIMFoam solver is based on version v2006 of OpenFOAM [41]. We can summarize the full implementation scheme of the REDIM method in OpenFOAM into the following steps:

- obtain the terms Ψ_θ^+, $D\Psi_\theta$ and Ψ_θ^+F by a simple linear interpolation method in the REDIM table depending on the generalized coordinates;
- calculate the m_s-dimensional vector $\nabla\theta$;
- compute the n-dimensional transport term $\nabla\cdot(D\Psi_\theta\cdot\nabla\theta)$ and the term for the reduced coordinate of the m_s-dimensional reduced manifold $\Psi^+\cdot\nabla\cdot(D\Psi_\theta\cdot\nabla\theta)$;
- supply the results of $\Psi_\theta^+\cdot\nabla\cdot(D\Psi_\theta\cdot\nabla\theta)$ and Ψ_θ^+F to Eq. (16) and solve the equation.

Finally, after solving Eq. (16) in each time step, a back-transformation of the solution $\theta(x_i, t)$ to $\Psi(\theta(x_i, t))$ is assigned by performing the linear interpolation in the REDIM lookup table [10, 36]. Note that the primary solution $\theta(x_i, t)$ is spatial profiles of the generalized coordinates. The thermo-chemical quantities (e.g. temperature, species mass fractions) can be retrieved by the back-transformation.

3.4. REDIMFoam based on physical coordinates

In the above section, we introduced the implementation of REDIM in generalized coordinates. It should be pointed out that the main disadvantage of using generalized coordinates to simulate combustion with REDIM is the lack of simple and transparent physical meaning. This means that it is difficult to interpret the obtained results. Therefore, some researchers [42, 17, 43] prefer to perform calculations in physical coordinates ξ which can be realized by a constant parametrization matrix C. The parametrization matrix defines a linear combination of variables in state space, $\xi = C\cdot\Psi$ [44]. For example, if the state vector consists of the following variables $\Psi = (h, p, \phi_{N_2}, \phi_{CO_2}, \phi_{CO}, \ldots, \phi_H)^T$, and the parametrization matrix is given by

$$C=\begin{bmatrix}0&0&1&0&0&\ldots&0\\0&0&0&1&0.5&\ldots&0\end{bmatrix},\quad \xi=\begin{pmatrix}\phi_{N_2}\\ \phi_{CO_2}+0.5\phi_{CO}\end{pmatrix}, \tag{17}$$

with the parameters $\xi_1 = \phi_{N_2}$ and $\xi_2 = \phi_{CO_2} + 0.5\phi_{CO}$. This simplifies post-processing of results and monitoring of the integration process. However, it can be challenging to find an appropriate monotonic parametrization that ensures a one-to-one mapping. This task is time-consuming, as it often involves searching for a suitable linear combination of the specific mole number of particular species [45].

A reduced model equation based on physical coordinates is established by analogy with the reduced equation in generalized coordinates (Eq. (14)) by using the chain rule and multiplying both sides with one matrix Ψ_ξ^+ [44]

$$\frac{\partial\xi}{\partial t}=\Psi_\xi^+\cdot F(\Psi(\xi))-U\cdot\nabla\xi-\frac{1}{\rho}\Psi_\xi^+\cdot\nabla\cdot\left(D\Psi_\xi\cdot\nabla\xi\right) \tag{18}$$

The reduced model equation for m_s-dimensional parametrization vector ξ is derived by combining Eq. (18) with the continuity equation

$$\frac{\partial(\rho\xi)}{\partial t}+\nabla\cdot(\rho U\cdot\xi)+\Psi_\xi^+\cdot\nabla\cdot\left(D\Psi_\xi\cdot\nabla\xi\right)=\rho\Psi_\xi^+\cdot F(\Psi(\xi)). \tag{19}$$

The matrix Ψ_ξ^+ can be expressed in terms of generalized coordinates, which can be computed by (details see Ref. [44])

$$\Psi_\xi^+=C\Psi_\theta\Psi_\theta^+. \tag{20}$$

The term $\Psi_\theta\Psi_\theta^+$ is a projector onto the tangent space of the manifold in generalized coordinates. This means that the matrix Ψ_ξ^+ can project the vector field onto the tangential subspace. The matrix Ψ_ξ can be defined as

$$\begin{aligned}\Psi_\xi &= \Psi_\theta\theta_\xi \\ &= \Psi_\theta\left(C\Psi_\theta\right)^{-1}.\end{aligned} \tag{21}$$

Therefore, the REDIM table based on generalized coordinates can be further post-processed, (for example, the terms $D\Psi_\xi = D\Psi_\theta(C\Psi_\theta)^{-1}$, $\Psi_\xi^+F = C\Psi_\theta\Psi_\theta^+F$), to get the REDIM table based on physical coordinates. Figure 6 shows the grid indices of a 2D REDIM table projected onto the (ξ_1, ξ_2) space, in which $\xi_1 = \phi_{N_2}$ and $\xi_2 = \phi_{CO_2} + 0.5\phi_{CO}$. The implementation scheme for the REDIM in physical coordinates is the same as the procedure in generalized coordinates. It simply entails replacing Eq. (16) with Eq. (19) in the reduced model equation that needs to be solved, as explained in the above section.

3.5. Evaluation of computational cost

The primary reason for utilizing low-dimensional manifolds in numerical combustion is to decrease computational costs. Consequently, it is necessary to compare the computational costs of the detailed simulations to the REDIM-based ones. To facilitate this comparison, the relative CPU time between detailed simulation and REDIM has been defined as [14],

$$\text{CPU time with REDIM} = \frac{\text{CPU time with REDIM}}{\text{CPU time with detailed mechanism}}, \tag{22}$$

where the CPU time denotes the computing time based on the same time step and mesh size with the detailed chemical kinetics and the REDIM reduced chemistry on a single CPU core. As introduced before, the REDIM reduced chemistry only solves ($3+m_s$) equations ($m_s \ll n_s$), which not only can significantly reduce the computational cost, but can efficiently decrease the stiffness of governing equations. Moreover, the thermo-chemical quantities are retrieved by the linear interpolation from a REDIM look-up table, which can avoid to solve highly non-linear chemical source terms.

4. Validation with 1D freely propagating flames

To verify the performance of the new REDIMFoam solver and to compare the results computed by the REDIM method in generalized and physical coordinates, an adiabatic 1D methane/air free flame is calculated in this section. The equivalence ratio (Φ) of the fuel mixture is $\Phi = 1$. A unity Lewis number is assumed. The boundary conditions used in the free flame are listed in Table 2, in which zero gradient denotes the Neumann boundary condition [46], and the others are Dirichlet boundary conditions [46]. A 1-dimensional REDIM (i.e. $m_s = 1$, ϕ_{CO_2} is selected here) is generated and provided to the REDIMFoam solver.

Table 2. Boundary conditions of the 1D free flame

	T	*p*	*U*	Species mass fractions
Left boundary	300 K	zero gradient	0.5 m/s	$\Phi = 1$
Right boundary	zero gradient	1 bar	zero gradient	zero gradient

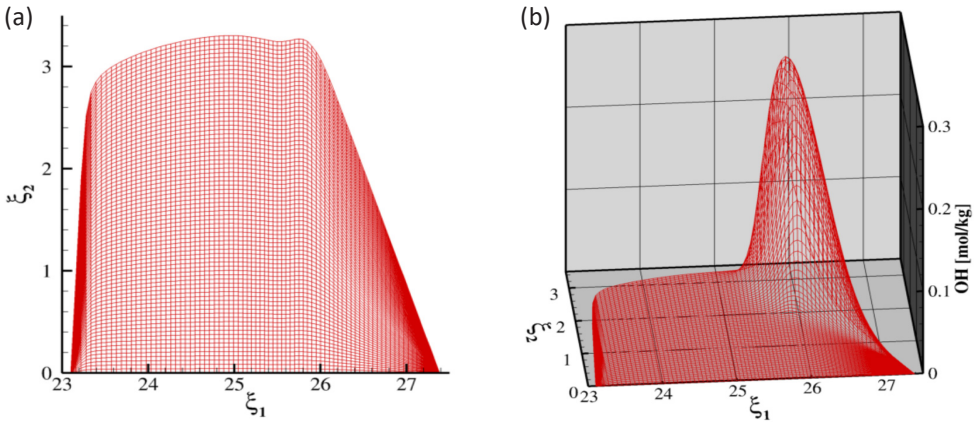

Fig. 6. Grid indices of a 2D REDIM table based on the physical coordinates, 2D projection of the manifold in the physical coordinates ξ (a), 3D projection of OH profile (b).

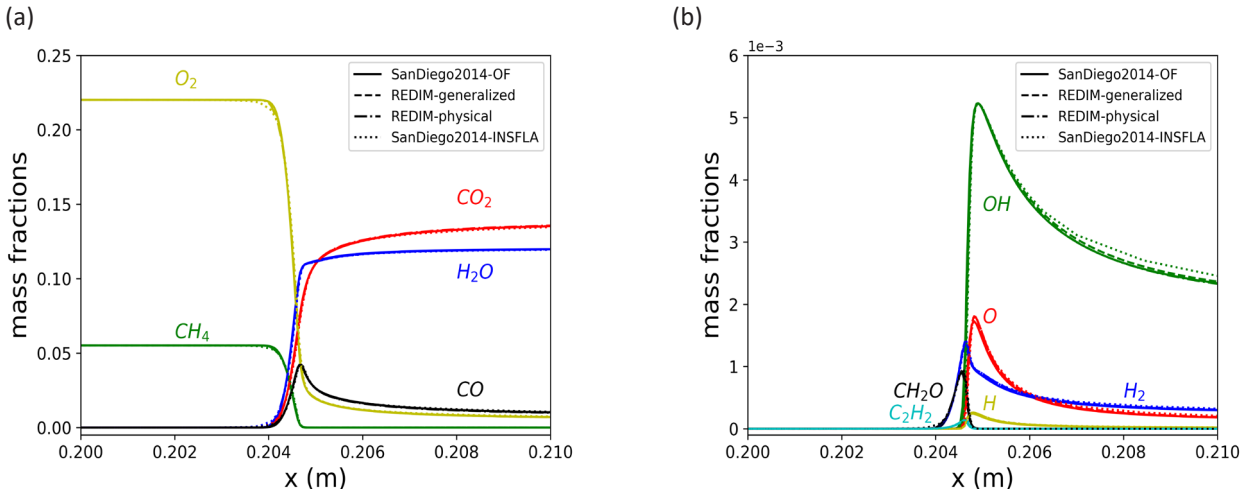

Fig. 7. Comparison of results for major (a) and minor (b) species computed with the SanDiego-2014 mechanism and the corresponding REDIM reduced chemistry in generalized and physical coordinates, solid line: EBIdnsFoam with SanDiego-2014, dashed line: REDIM in generalized coordinate, dashed dotted line: REDIM in physical coordinate, dotted line: INSFLA with SanDiego-2014.

The computational results obtained with the detailed mechanism (SanDiego-2014 mechanism [47] used in EBIdnsFoam and INSFLA) and the corresponding REDIM reduced chemistry (used in REDIMFoam) are compared. In Fig. 7, some major and minor species are plotted over the spatial coordinate. A good agreement can be observed between the results obtained from EBIdnsFoam and INSFLA code with the same mechanism. It can also be seen that an accurate description of these species profiles can be obtained with the REDIM method comparing with the detailed solutions (EBIdnsFoam and INSFLA code), even for minor species. The computed results with 1D REDIM in the generalized coordinate are slightly different from these results in the physical coordinate. Moreover, Strassacker et al. calculated a head-on quenching flame with the 2D REDIM in generalized and physical coordinates, and found nearly no discrepancy between the results with generalized and physical coordinates [44].

The CPU time of the detailed simulation with the EBIdnsFoam solver is 4.49 s, however, the CPU time of REDIMFoam in generalized and physical coordinates are 0.51 s and 0.55 s, respectively. The relative CPU time of REDIM in generalized and physical coordinates is approximately 11% and 12% of the detailed mechanism, showing a significant reduction in simulation time.

The calculated results based on the generalized coordinate have excellent agreement with the corresponding results computed by using the physical coordinate, and the CPU time is almost the same. The generalized coordinate can improve the efficiency and the robustness of interpolation calculation during the implementation of REDIM, since the structure of the grid is locally orthogonal and equidistant everywhere [36]. Therefore, we will use the REDIMFoam solver based on generalized coordinates for the following simulations in this paper.

5. Validation using 2D counterflow flames

5.1. Problem definition

In order to verify the REDIM-based solver, results computed by the finite rate chemistry and REDIM methods are compared in this section. The flame studied is a two-dimensional axisymmetric laminar counterflow flame. A stream of methane mixed with air (25% CH_4 + 75% air in volume percent, $\Phi = 3.17$) is injected from the left boundary while a stream of air (21% O_2 + 79% N_2 in volume percent) is injected from the right boundary. The mixture composition is the same as the composition used in the Sandia flame [48], and the simulation of 1D counterflow diffusion flames based on the fuel mixture has been investigated in the steady and unsteady regimes [14]. In this paper, we mainly study the properties of 2D counterflow diffusion flames with detailed and reduced mechanisms. Gravity and radiation are neglected in the calculations. A brief schematic of the burner configuration is presented in Fig. 8, which is similar to the burner geometry in Refs. [49, 50]. The geometry has been simplified to make it easier to simulate in this work, namely not considering the nozzle rim thickness and the nozzle protrusion length.

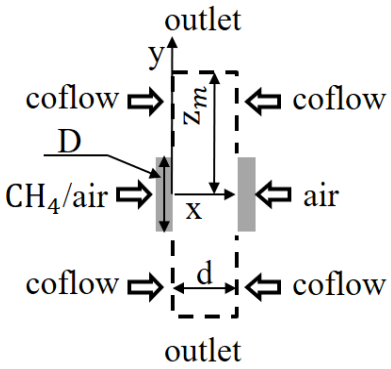

Fig. 8. Schematic of the burner configuration and axisymmetric computational domain.

5.2. Numerical setup

5.2.1. Computational domain and mesh size

The computational domain is axisymmetric (2-dimensional), and diameters of the nozzles (*D*) for the fuel flow and the oxidizer flow are both 2 cm. The distance *d* between the two nozzles is 2 cm as well, in addition, the computational height is z_m = 4 cm (measured from the centerline of the nozzle).

In the present work, three mesh resolutions (mesh 1, mesh 2 and mesh 3 listed below) are used to compute the 2D axisymmetric laminar flames with the detailed mechanism and the corresponding REDIM method, respectively, in order to investigate the mesh dependence. In the computational domain between the two nozzles (2 cm x 2 cm), the mesh is equidistantly spaced along both x and y directions (see Fig. 8), but out of this domain, the mesh size increases proportionally in the y direction.

- Mesh 1 (coarse):
  Δx = 0.1 mm for $0 \le x \le 2$ cm, Δy = 0.25 mm for $0 \le y \le 1$ cm, and increasing spacing starting from Δy = 0.26 mm for $1 < y \le 4$ cm.
- Mesh 2 (fine):
  Δx = 0.05 mm for $0 \le x \le 2$ cm, Δy = 0.125 mm for $0 \le y \le 1$ cm, and increasing spacing starting from Δy = 0.13 mm for $1 < y \le 4$ cm.
- Mesh 3 (very fine):
  Δx = 0.025 mm for $0 \le x \le 2$ cm, Δy = 0.125 mm for $0 \le y \le 1$ cm, and increasing spacing starting from Δy = 0.13 mm for $1 < y \le 4$ cm.

5.2.2. Boundary conditions and mechanisms

The boundary conditions considered for the 2D counterflow flames are listed in Table 3. The inlet velocities are equal in magnitude and opposite in direction for both nozzle streams, which are set to different values (details are discussed in the following sections). Air flows from the concentric pipe (coflow) with an axial velocity of 0.01 m/s [49]. The outlet is treated as an outflow boundary condition.

The detailed mechanisms GRI 3.0 [51] and SanDiego-2014 [47] are used in the simulations with the EBIdnsFoam solver, which consist of 53 species with 325 reactions and 48 species with 247 reactions, respectively. The assumption of unity Lewis number is used in this case, which has been shown to be a reasonable simplification in these kind of flame configurations [52, 53, 54], although REDIM can handle the detailed transport, too [34]. Furthermore, the focus of the work is not an analysis of the transport model, but a comparison between detailed and reduced chemistry.

The 2D REDIM reduced chemistry (m_s = 2) is applied to calculate the 2D counterflow flames. The boundary conditions and initial conditions used for the generation of REDIM are taken from a collection of 1D counterflow flames with different strain rates (a = 80, 100, 120, 140, 160, 180, 200, 300 s^{-1} and mixing line) computed with the GRI3.0 and SanDiego-2014 mechanisms, in which the flamelet with low strain rate of 80 s^{-1} is the upper boundary and the mixing line represents the lower boundary of the application range of REDIM. The assumption of unity Lewis number is also used in the REDIM method.

5.3. Mesh dependence

The computational results with the detailed mechanism (GRI3.0) and the corresponding REDIM method are presented in this section in order to investigate the influence of different mesh resolutions on flame structure. The detailed solutions are computed by the EBIdnsFoam solver and the reduced results are calculated by the REDIMFoam solver based on the generalized coordinate. The inlet velocity of the counterflow nozzles is set to 1.0 m/s. $\phi = (\phi_{N_2}, \phi_{CO_2})^T$ is selected as the progress variables in this section.

Table 3. Boundary conditions of 2D counterflow flame

	T	*p*	*U*	Species mass fractions
Nozzles	293 K	zero gradient	fixed	25% CH_4 + 75% air
Coflow	293 K	zero gradient	0.01 m/s	air
Outlet	zero gradient	1 bar	zero gradient	zero gradient

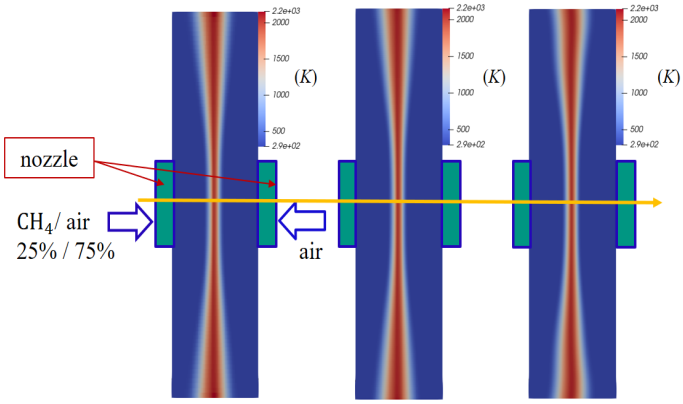

Fig. 9. Temperature profiles computed by the EBIdnsFoam with the GRI3.0 mechanism on three mesh sizes, left figure: mesh 1; middle figure: mesh 2; right figure: mesh 3; the yellow line marks the centerline along the computational domain.

Figure 9 shows the structures of two dimensional axisymmetric laminar diffusion flames computed with the GRI3.0 mechanism, in which green rectangles denote the location of nozzles, not belonging to the computational domain. Figures 10a and 10b display contours of temperature and profiles of selected species mass fractions along the centerline of the computational domain on three mesh sizes, respectively. As can be observed, the peak temperatures (black line: 2006 K on mesh 1; red line: 2016 K on mesh 2; blue line: 2019 K on mesh 3) computed on the three meshes have almost the same values, and the error is very small. The minor species profiles (OH and O mass fractions) computed by mesh 1 show some differences to the finer meshes (mesh 2 and mesh 3), while the results between mesh 2 and mesh 3 show good agreement in Fig. 10b.

In Fig. 11a, it is shown that the flame thickness computed by mesh 1 is a bit larger than the results on mesh 2 and mesh 3, while the error is less than 2%. Although the peak temperatures on mesh 1 (black line: 1992 K) is slightly lower than the values (red line: 2015 K; blue line: 2017 K). On mesh 2 and mesh 3, the error is very small as well. Similar conclusions are drawn regarding the minor species profiles in Fig. 11b. Therefore, mesh 2 is sufficient to capture the flame structure for the detailed and reduced chemistry, and will be used in the following. On mesh 2 and mesh 3, the error is very small as well. Similar conclusions are drawn regarding the minor species profiles in Fig. 11b. Therefore, mesh 2 is sufficient to capture the flame structure for the detailed and reduced chemistry, and will be used in the following.

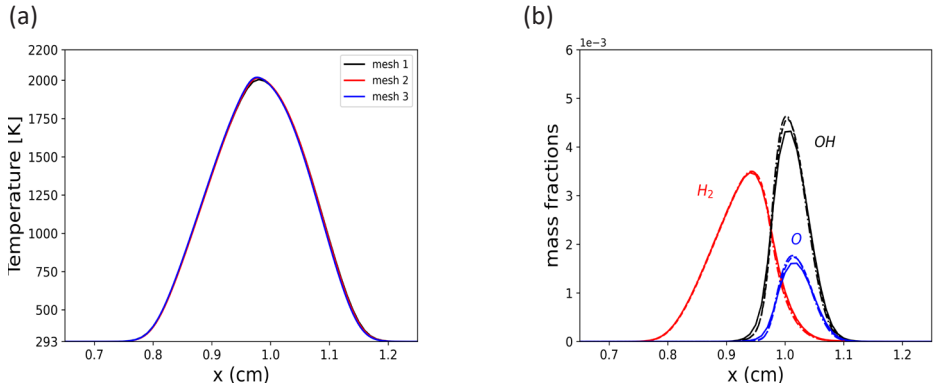

Fig. 10. Comparison of results for temperature (a) and minor species (b) computed by the EBIdnsFoam with the GRI3.0 mechanism along the centerline of the 2D counterflow flame on three mesh sizes, solid line: mesh 1, dashed line: mesh 2, dashed dotted line: mesh 3.

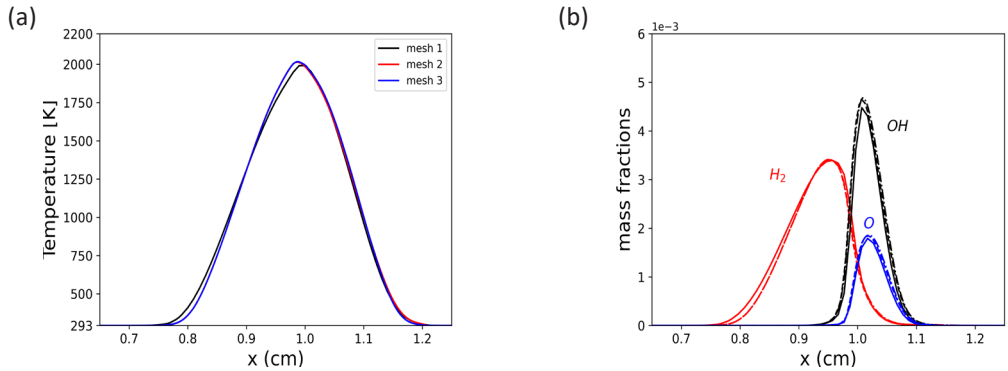

Fig. 11. Comparison of results for temperature (a) and minor species (b) computed by REDIMFoam along the centerline of the 2D counterflow flame on three mesh sizes, solid line: mesh 1, dashed line: mesh 2, dashed dotted line: mesh 3.

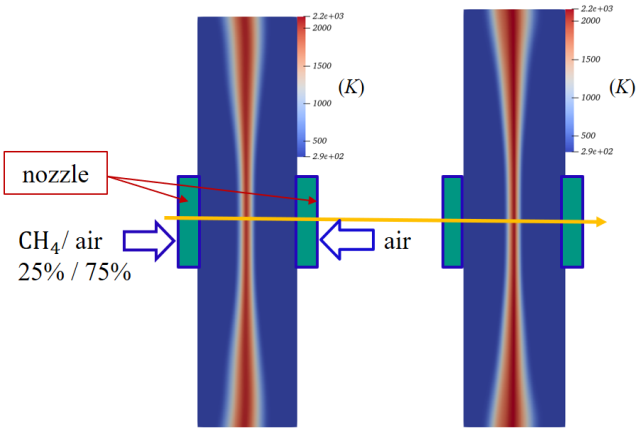

Fig. 12. Temperature profiles on mesh 2, left figure: EBIdnsFoam; right figure: RED-IMFoam; the yellow line marks the centerline along the computational domain.

5.4. Influence of the choice of progress variable

In this section, two different linear combinations of parametrization ($\phi = (\phi_{N_2}, \phi_{CO_2})^T$ and $(\phi_{N_2}, \phi_{CO_2} + 0.5\phi_{CO})^T$) have been chosen to verify the in- variance of the REDIM method on the choice of progress variable. The inlet velocity of the nozzles is 1.0 m/s. The GRI3.0 mechanism is used in the section. Figure 12 shows the temperature profiles of the 2D counterflow flames, in which the left part of each sub-figure in Fig. 12 shows the results obtained by the EBIdnsFoam using the detailed chemistry (GRI 3.0), while the right part shows the results computed by the REDIMFoam with (ϕ_{N_2}, ϕ_{CO_2}) progress variables.

As can be seen in Fig. 13, the results of the RED-IM reduced model obtained with different progress variables (ϕ_{N_2}, ϕ_{CO_2}) and (ϕ_{N_2}, ϕ_{CO_2} + .5ϕ_{CO}), both are almost the same as detailed simulation results, in terms of temperature or H_2O mass fraction, and even for the minor species such as OH mass fraction. Although the mass fraction of O computed by the REDIM method is slightly different to the detailed solution of the EBIdnsFoam, the profiles computed by the REDIMFoam with the two different progress variables are nearly the same. The peak temperature computed by the detailed simulation is 2016 K, while the values obtained with the progress variables (ϕ_{N_2}, ϕ_{CO_2}) and (ϕ_{N_2}, ϕ_{CO_2} + 0.5ϕ_{CO}) are 2015 K and 2016 K respectively in Fig. 13a, which shows that the generation of the REDIM reduced chemistry is independent on the choice of the progress variable, as long as a one-to-one mapping of REDIM is guaranteed, as discussed in section 3.1.

5.5. Influence of the choice of reaction mechanism

In this section, we want to study an interesting question: Is the difference between REDIMFoam and EBIdnsFoam for the same mechanism or is the differ-

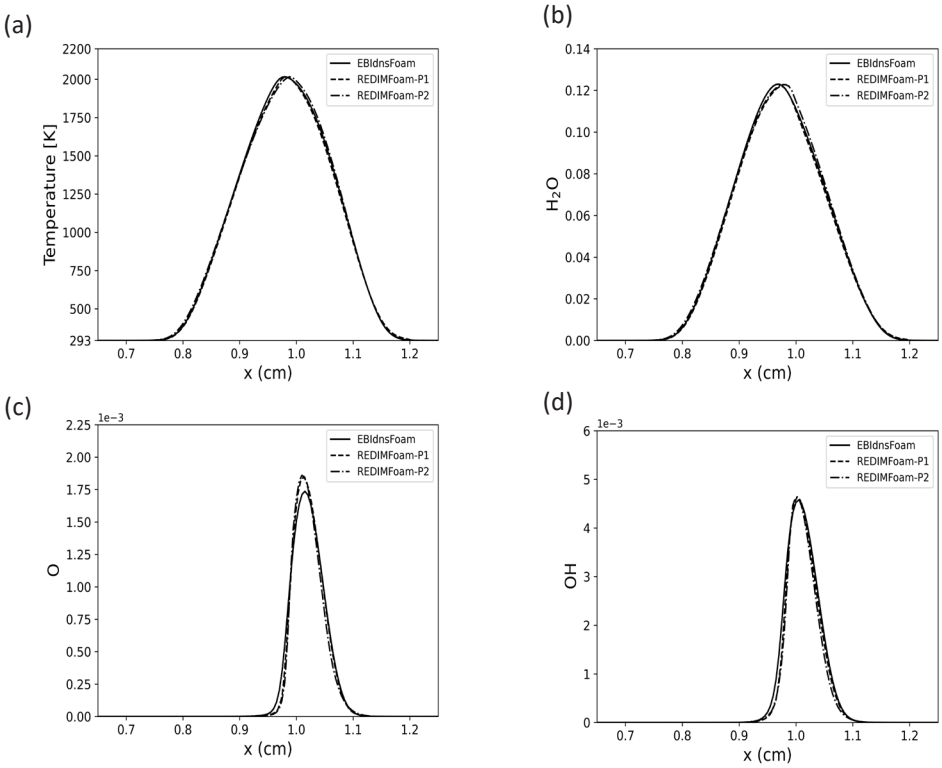

Fig. 13. Comparison of results for temperature (a) and mass fractions of H_2O (b), O (c) and OH (d) along the centerline of the 2D counterflow flame, solid line: EBIdns-Foam, dashed line (REDIMFoam-P1): (ϕ_{N_2}, ϕ_{CO_2}), dashed dotted line (REDIMFoam-P2): (ϕ_{N_2}, ϕ_{CO_2} + 0.5ϕ_{CO}).

ence between different mechanisms larger? Therefore, the computational results obtained with the detailed mechanisms (GRI 3.0 and SanDiego-2014) and the REDIM reduced chemistry are compared in the section on mesh 2. Two REDIM tables are generated by two detailed mechanisms, the GRI 3.0 mechanism and the SanDiego-2014 mechanism. The inlet velocity of the two streams is 1.0 m/s. $\phi = (\phi_{N_2}, \phi_{CO_2})$ is selected as the progress variable in this section.

The profiles of temperature and selected species mass fractions over N_2 mass fraction for two detailed mechanisms (GRI3.0 and SanDiego-2014) as well as their corresponding REDIMs (dashed line) are shown in Fig. 14. The temperature and mass fraction of CO_2 over N_2 mass fraction is quantitatively similar for the two mechanisms. The peak temperature (2015 K in Fig. 14a) obtained from the REDIM reduced mechanism is close to the peak temperature (2016 K) computed by the EBIdnsFoam with the GRI3.0 mechanism, moreover, the peak temperature (2031 K) calculated by the SanDiego-2014 mechanism is 2032 K in the REDIM reduced chemistry. The errors introduced by REDIM are less than 0.1%. The maximum of CO_2 mass fractions shows negligible differences between the detailed mechanisms and the REDIM reduced model as well. This means that the REDIM method can reproduce the structure of the 2D counterflow flame accurately. In contrast, the profiles of minor species O and OH over N_2 mass fraction are different for the two mechanisms. It is shown that the differences between REDIMFoam and EBIdnsFoam for the same mechanism are much smaller than the ones between the different mechanisms. Consequently, the computation with REDIM reduced chemistry shows excellent agreement with corresponding results computed by the different detailed mechanisms.

5.6. Influence of the inlet velocity

5.6.1. Model performance under steady conditions

This section investigates the behavior of REDIM for various inlet velocities of the nozzle which are commonly used to determine global strain rates a_g in 2D counterflow flames. The definition of the global strain rate is as follows [50, 49, 55]

$$a_g = \frac{2U_r U_F}{d}\left(1+\frac{\sqrt{\rho_F}}{U_r\sqrt{\rho_O}}\right), \tag{23}$$

where the velocity ratio $U_r = U_O/U_F$, U_O and U_F denote the inlet velocities of the air and fuel streams, d is the distance between two nozzles in Fig. 8, and ρ_F and ρ_O are the density of fuel mixture and air, respectively. The values of the inlet velocity for fuel and air streams at both nozzles are same in this work, therefore $U_r = 1$, $U_F = U$.

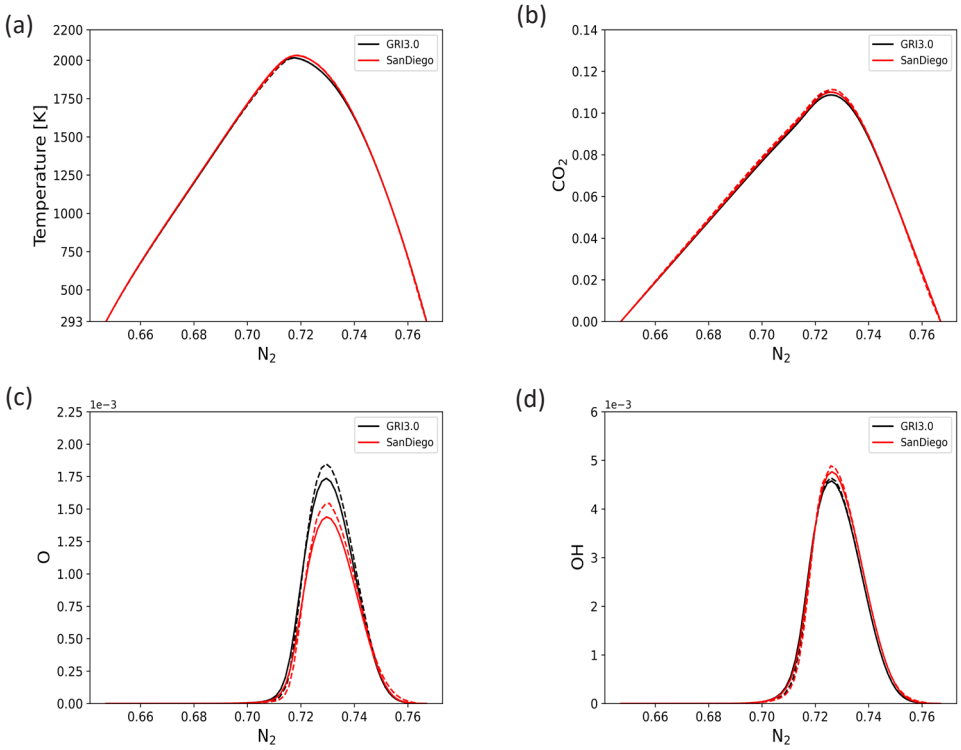

Fig. 14. Comparison of results for temperature (a) and mass fractions of CO_2 (b), O (c) and OH (d) over mass fraction N_2 with detailed (solid line) and reduced (dashed line) mechanisms along the centerline of the 2D counterflow flame.

Table 4. Peak temperatures

Inlet velocity	Global strain rate	EBIdnsFoam	REDIMFoam
U = 0.5 m/s	a_g = 97 s^{-1}	2043 K	2038 K
U = 1.0 m/s	a_g = 194 s^{-1}	2016 K	2015 K
U = 1.5 m/s	a_g = 291 s^{-1}	1997 K	1987 K

The REDIM is based on the GRI3.0 mechanism. ϕ = (ϕ_{N_2}, ϕ_{CO_2}) is selected as the progress variable. Figure 15a shows the temperature profiles calculated by the EBIdnsFoam with the GRI3.0 mechanism and the REDIMFoam at three different inlet velocities (U = 0.5, 1.0 and 1.5 m/s). Comparing the temperature profiles of the detailed chemistry and the REDIM method, it is found that the REDIM can reproduce the flame structure very well with the change of inlet velocity and strain rate. The peak temperatures of the detailed mechanism decrease with the increase of the inlet velocity in Table 4, and the peak temperatures computed by the REDIM method have the same tendency with the change of the inlet velocity.

Figure 15b shows the profiles of mass fractions for major species (H_2O). Analyzing the computational results, we found that the results obtained by the REDIM method have a better agreement with those obtained by the detailed chemistry. The maxima of H_2O computed by the REDIM method are approximately equal to the values computed by the detailed mechanism. As for the minor species, OH and H_2, the results computed by the REDIM method still have a good agreement with the results from the detailed mechanism in Figs. 15c and 15d.

The maximum of temperature and mass fractions of major and minor species along the centerline of the 2D counterflow flame computed by the EBIdnsFoam and the REDIMFoam over strain rates (that is, different inlet velocities) from 97 s^{-1} to 972 s^{-1} are compared in Fig. 16. We can see that the results computed by the REDIM method agree well with the detailed chemistry in the range of small global strain rates (97–600 s^{-1}). Small differences can be observed in the maximum of minor species, e.g. OH at larger global strain rates (> 600 s^{-1}), while the values of temperature and H_2O mass fraction in the REDIM

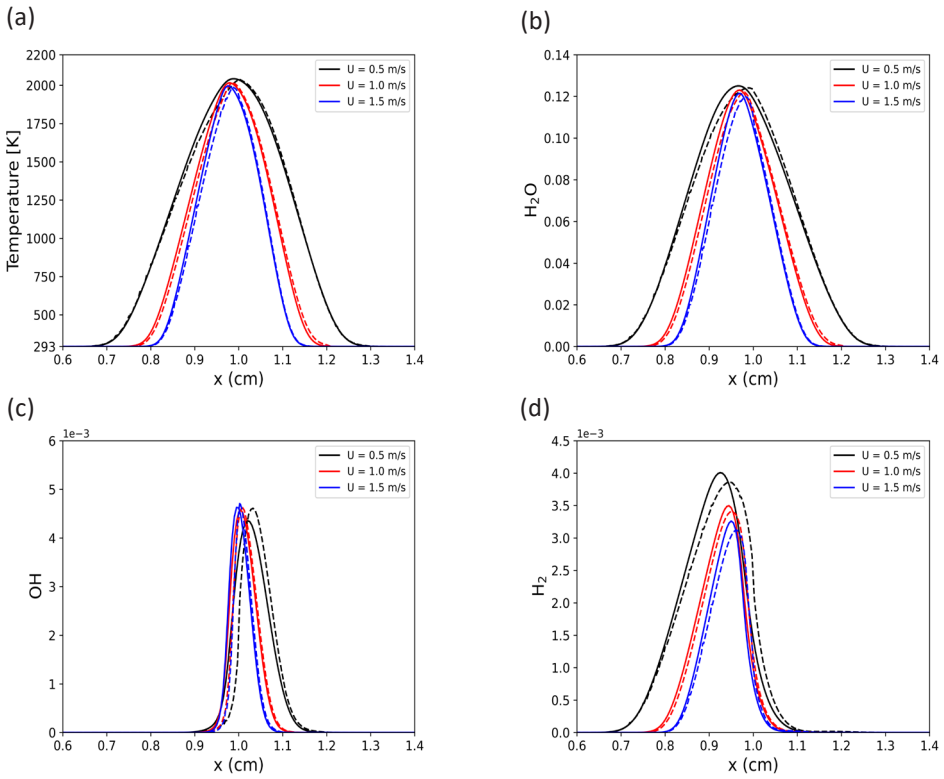

Fig. 15. Comparison of results for temperature (a) and mass fractions of H_2O (b), OH (c) and H_2 (d) along the centerline of the 2D counterflow flame at three different inlet velocities (U = 0.5, 1.0 and 1.5 m/s), solid line: EBIdnsFoam, dashed line: REDIMFoam.

method show good agreement with results of the detailed chemistry for all strain rates. The difference of minor species between the detailed and REDIM simulations can be improved by using higher dimensional manifolds.

5.6.2. Model performance under extinction conditions

In the preceding sections, our focus was solely on validating REDIM's performance under steady state conditions. By increasing the global strain rate beyond the quenching limit (1457 s^{-1}), we not investigate whether the REDIM method can provide an accurate description of the flame response. This scenario offers an intriguing test case to assess REDIM's performance in dealing with extinction conditions. Hence, we employ a time-varying step function to elevate the global strain rate from 97 s^{-1} to above the quenching limit of 1550 s^{-1}. Figure 17 shows the temperature and OH mass fraction profiles along the centerline during the extinction process with the GRI3.0 mechanism in the 2D counterflow flame. As can be seen in Fig. 17b, the global strain rate exceeds the flame quenching limit for less than 2 ms, which leads to the flame extinguishing.

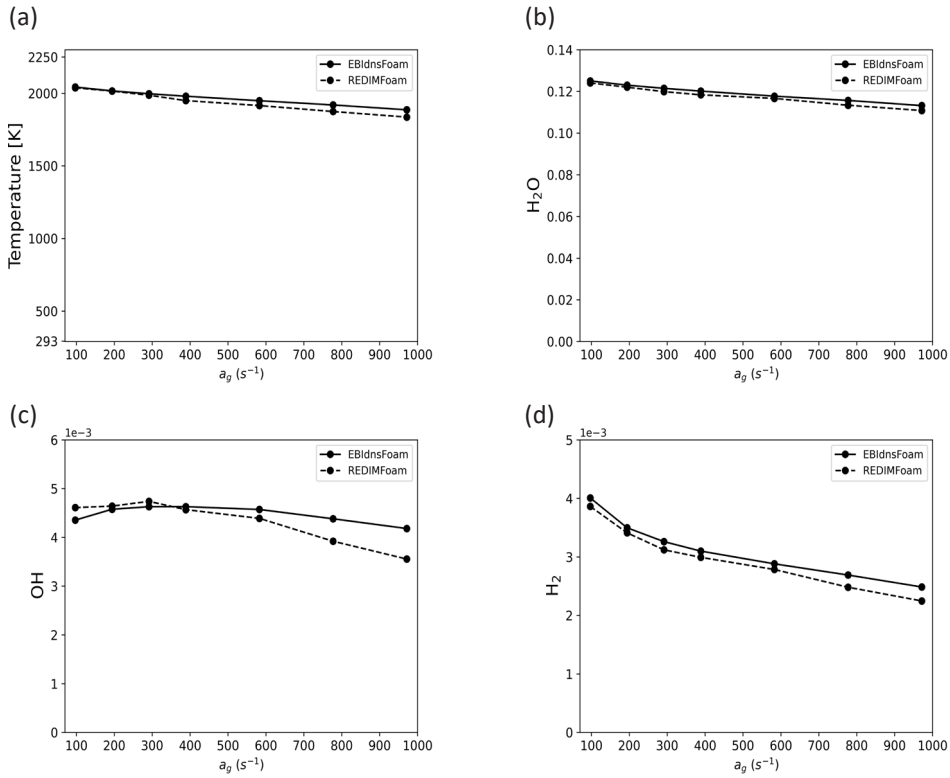

Fig. 16. Comparison of results for maxima of temperature (a) and mass fractions of H_2O (b), OH (c) and H_2 (d) along the centerline of the 2D counterflow flame over global strain rates, solid line: EBIdnsFoam, dashed line: REDIMFoam.

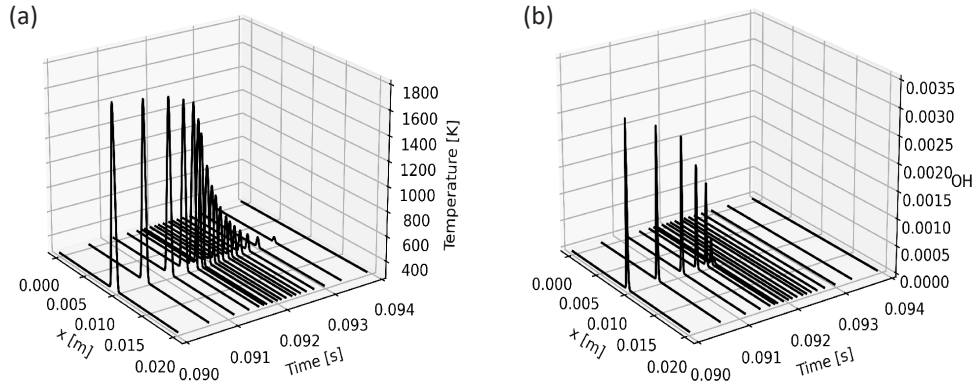

Fig. 17. Temperature and OH mass fraction profiles during the extinction process with detailed mechanism in the 2D counterflow flame.

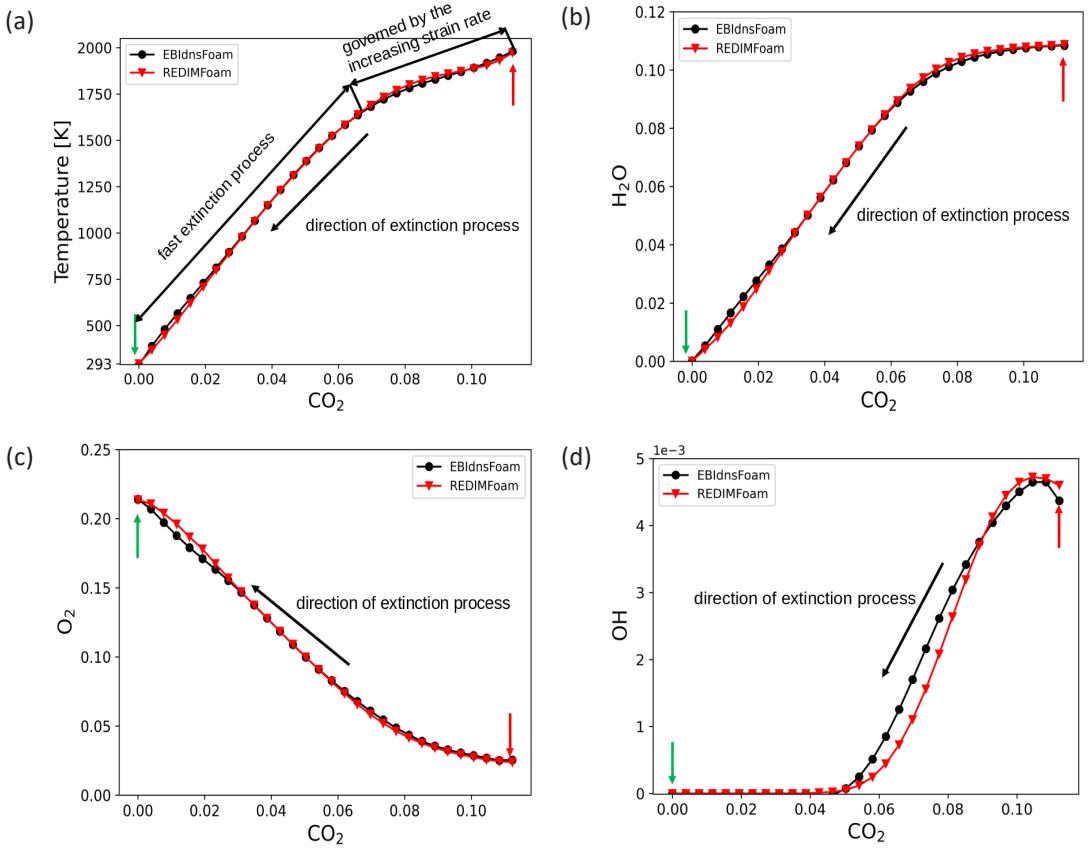

Fig. 18. Comparison of the extinction process in the 2D counterflow flame, black line: EBIdnsFoam, red line: REDIMFoam.

Figure 18 illustrates the state space of temperature and mass fractions of H_2O, O_2 and OH over mass fraction of CO_2, as calculated by the EBIdnsFoam using the GRI3.0 mechanism (black line) and the REDIMFoam (red line) at the point of maximum CO_2 mass fraction during the extinction process. The points indicated by red arrows denote the initial state and the points indicated by green arrows are extinguished states. The black arrows show the direction of the extinction process. The extinction process can be divided into two parts, one is governed by the increasing strain rate, and the other is the fast extinction process after reaching the quenching limit. Regarding the REDIM solutions, it is evident that, by definition, their movement is constrained within the REDIM slow manifolds. It can be observed that the REDIM reduced chemistry can describe the behaviour of extinction in the flames very well, even though we do not explicitly provide the extinction flamelets in the generation of REDIM. The results of temperature and mass fractions of H_2O and O_2 with the REDIM reduced chemistry almost overlap with the detailed solution. This implies that these thermokinetic properties exhibit changes in close proximity to the manifold during the extinction process. Although there is a minor discrepancy for the OH mass fraction between detailed and reduced solutions during the extinction process in Fig. 18d, the REDIM method still clearly shows the evolution of the extinction process with acceptable accuracy in the 2D counterflow flames.

6. Conclusions

In this paper, the REDIM method has been implemented into a new OpenFOAM-based CFD solver, REDIMFoam, and was applied to different premixed and diffusion flame configurations. The work focuses on evaluating the performance of the REDIM method in steady and transient flames, both in terms of prediction accuracy and computational efficiency. The REDIM method considers both the chemical reaction effect and the coupling of molecular transport with thermochemical processes in generating a low dimensional manifold, that can be applied to different combustion scenarios. Therefore, the REDIM approach can be used in simulations where convection and diffusion have a greater impact on the combustion process, specifically in the low-temperature combustion region. The results indicate

that the REDIM-based solver performs very well for both steady and transient processes. Remarkably, the REDIM model can effectively capture the flame dynamics, including extinction events.

The use of generalized and physical coordinates for the REDIM has been investigated by simulating an adiabatic 1D premixed methane/air free flame. The calculated results based on generalized coordinates show excellent agreement with their corresponding results in physical coordinates, and the CPU time is almost the same. Due to the efficiency and the robustness of interpolation during the implementation of REDIM in generalized coordinate, using generalized coordinate is generally recommended.

The REDIM-based chemistry is further used to calculate 2D counterflow diffusion flames. The results of the REDIM model obtained with different progress variables are almost the same as the results from detailed chemistry simulations, which confirms that the REDIM method is independent of the choice of the progress variables. Results from the REDIM method are compared for two different detailed mechanisms and show good agreement with the detailed solution, even for most of the minor species. The differences between the REDIM approach and the detailed chemistry are much smaller than the ones between the different mechanisms. The REDIM method can reproduce the flame structure under different global strain rates. It is shown that the 2D REDIM can describe the flame structures of steady and quenching regimes in the 2D counterflow flames very well, while the standard steady flamelet method needs additional extinction regimes to do this. Furthermore, the REDIM method has the significant advantage of reducing the computational cost by one order of magnitude compared to the detailed simulations. All the above conclusions could also be drawn in the case of turbulent flames [17, 56, 22].

Acknowledgments

We thank Dr. Viatcheslav Bykov and Dr. Chunkan Yu for useful discussion about the implementation of REDIM.

References

[1]. J. Warnatz, U. Maas, R.W. Dibble, Combustion: Physical and Chemical Fundamentals, Modeling and Simulation, Experiments, Pollutant Formation, Berlin: Springer, 2006.

[2]. J.A. van Oijen, A. Donini, R.J.M. Bastiaans, et al., State-of-the-art in premixed combustion modeling using flamelet generated manifolds, *Prog. Energy Combust. Sci.* 57 (2016) 30–74. DOI: 10.1016/j.pecs.2016.07.001

[3]. F.A. Williams, Combustion Theory, 2nd Edition, Westview Press, 1985.

[4]. M. Rein, The partial-equilibrium approximation in reacting flows, *Phys. Fluids* 4 (1992) 873–886. DOI: 10.1063/1.858267

[5]. U. Maas, S.B. Pope, Simplifying chemical kinetics: Intrinsic low-dimensional manifolds in composition space, *Combust. Flame* 88 (1992) 239–264. DOI: 10.1016/0010-2180(92)90034-M

[6]. S. Lam, D. Goussis, Understanding complex chemical kinetics with computational singular perturbation, *Proc. Combust. Inst.* 22 (1989) 931–941. DOI: 10.1016/S0082-0784(89)80102-X

[7]. O. Gicquel, N. Darabiha, D. Thévenin, Liminar premixed hydrogen/air counterflow flame simulations using flame prolongation of ILDM with differential diffusion, *Proc. Combust. Inst.* 28) (2000) 1901–1908. DOI: 10.1016/S0082-0784(00)80594-9

[8]. V. Bykov, U. Maas, Extension of the ILDM method to the domain of slow chemistry, *Proc. Combust. Inst.* 31 (2007) 465–472. DOI: 10.1016/j.proci.2006.08.104

[9]. J.A. van Oijen, L.P.H. de Goey, Modelling of premixed laminar flames using flamelet-generated manifolds, *Combust. Sci. Technol.* 161 (2000) 113–137. DOI: 10.1080/00102200008935814

[10]. V. Bykov, U. Maas, The extension of the ILDM concept to reaction–diffusion manifolds, *Combust. Theory Model.* 11 (2007) 839–862. DOI: 10.1080/13647830701242531

[11]. V. Bykov, A. Neagos, U. Maas, On transient behavior of non-premixed counter-flow diffusion flames within the REDIM based model reduction concept, *Proc. Combust. Inst.* 34 (2013) 197–203. DOI: 10.1016/j.proci.2012.06.073

[12]. A. Neagos, V. Bykov, U. Maas, Study of extinction limits of diluted hydrogen-air counter-flow diffusion flames with the REDIM method, *Combust. Sci. Technol.* 186 (2014) 1502–1516. DOI: 10.1080/00102202.2014.935125

[13]. P. Golda, A. Blattmann, A. Neagos, et al., Implementation problems of manifolds-based model reduction and their generic solution, *Combust. Theory Model.* 24 (2020) 377–406. DOI: 10.1080/13647830.2019.1682198

[14]. C. Yu, F. Minuzzi, U. Maas, REDIM reduced chemistry for the simulation of counterflow diffusion flames with oscillating strain rates,

Combust. Theory Model. 24 (2020) 682–704. DOI: 10.1080/13647830.2020.1739336

[15]. K. Koenig, V. Bykov, U. Maas, Investigation of the dynamical response of methane/air counterflow flames to inflow mixture composition and flow field perturbations, *Flow Turbulence Combust.* 83 (2009) 105–129. DOI: 10.1007/s10494-008-9191-x

[16]. R. De Meester, B. Naud, U. Maas, B. Merci, Transported scalar PDF calculations of a swirling bluff body flame ('SM1') with a reaction diffusion manifold, *Combust. Flame* 159 (2012) 2415–2429. DOI: 10.1016/j.combustflame.2012.01.026

[17]. P. Wang, F. Zieker, R. Schießl, et al., Large eddy simulations and experimental studies of turbulent premixed combustion near extinction, *Proc. Combust. Inst.* 34 (2013) 1269–1280. DOI: 10.1016/j.proci.2012.06.149

[18]. C.J. Greenshields, OpenFOAM User Guide (version 7), CFD Direct Ltd. (2019).

[19]. Y. Luo, C. Strassacker, F. Ferraro, et al., A manifold-based reduction method for side-wall quenching considering differential diffusion effects and its application to a laminar lean dimethyl ether flame, *Int. J. Heat Fluid Flow* 97 (2022) 109042. DOI: 10.1016/j.ijheatfluidflow.2022.109042

[20]. Y. Luo, C. Strassacker, U. Maas, C. Hasse, Model reduction on the fly: Simultaneous identification and application of reduced kinetics for the example of flame-wall interactions, *Proc. Combust. Inst.* 39 (2023) 5239–5248. DOI: 10.1016/j.proci.2022.07.227

[21]. P. Shrotriya, R. Schiessl, C. Yu, et al., An iterative methodology for redim reduced chemistry generation and its validation for partially-premixed combustion, *Combust. Theory Model*. 28 (2024) 65–98. DOI: 10.1080/13647830.2023.2260350

[22]. P. Shrotriya, R. Schiessl, V. Bykov, U. Maas, LES of turbulent partially-premixed flames using reaction–diffusion manifold-reduced chemistry with a consistent gradient estimate determined "on the fly", *Proc. Combust. Inst.* 40 (2024) 105273. DOI: 10.1016/j.proci.2024.105273

[23]. N. Li, Application of reaction-diffusion manifolds (REDIM) for the simulation of laminar diffusion flames, PhD dissertation, Karlsruhe Institute of Technology (2024).

[24]. T.J. Poinsot, D.P. Veynante, (2004). Combustion. In Encyclopedia of Computational Mechanics (eds E. Stein, R. Borst and T.J.R. Hughes). DOI: 10.1002/0470091355.ecm067

[25]. T. Zirwes, F. Zhang, P. Habisreuther, et al., Quasi-DNS dataset of a piloted flame with inhomogeneous inlet condi tions, *Flow Turbulence Combust.* 104 (2020) 997–1027. DOI: 10.1007/s10494-019-00081-5

[26]. T. Zirwes, M. Sontheimer, F. Zhang, et al., Assessment of numerical accuracy and parallel performance of OpenFOAM and its reacting flow extension EBIdnsFoam, *Flow Turbulence Combust.* 111 (2023) 567–602. DOI: 10.1007/s10494-023-00449-8

[27]. J.O. Hirschfelder, C.F. Curtiss, R.B. Bird, Molecular Theory of Gases and Liquids, John Wiley & Sons, 1964.

[28]. R.J. Hall, The radiative source term for plane-parallel layers of reacting combustion gases, *J. Quant. Spectrosc. Radiat. Transfer* 49 (1993) 517–523. DOI: 10.1016/0022-4073(93)90064-O

[29]. R.J. Hall, Radiative dissipation in planar gas-soot mixtures, *J. Quant. Spectrosc. Radiat. Transfer* 51 (1994) 635–644. DOI: 10.1016/0022-4073(94)90117-1

[30]. W.L. Grosshandler, RADCAL: A narrow-band model for radiation calculations in a combustion environment, Tech. Rep. Nr. 1402, National Institute of Standards and Technology (1993). DOI: 10.6028/NIST.TN.1402

[31]. D.G. Goodwin, R.L. Speth, H.K. Moffat, B.W. Weber, Cantera: An object-oriented software toolkit for chemical kinetics, thermodynamics, and transport processes, Version 2.5.1, 2021. Available: https://zenodo.org/records/4527812?utm_source=.com

[32]. C. Yu, P. Shrotriya, X. Li, U. Maas, Reduced modeling of the nox formation based on the reaction-diffusion manifolds method for counterflow diffusion flames, *Proc. Combust. Inst.* 39 (2023) 1587–1596. DOI: 10.1016/j.proci.2022.08.010

[33]. U. Maas, D. Thévenin, Correlation analysis of direct numerical simulation data of turbulent non-premixed flames, *Proc. Combust. Inst.* 27 (1998) 1183–1189. DOI: 10.1016/S0082-0784(98)80521-3

[34]. U. Maas, V. Bykov, The extension of the reaction/diffusion manifold concept to systems with detailed transport models, *Proc. Combust. Inst.* 33 (2011) 1253–1259. DOI: 10.1016/j.proci.2010.06.117

[35]. U. Maas, J. Warnatz, Ignition processes in hydrogen-oxygen mixtures, *Combust. Flame* 74 (1988) 53–69. DOI: 10.1016/0010-2180(88)90086-7

[36]. J. Bauer, V. Bykov, U. Maas, Implementation of ILDMs based on a representation in generalized coordinate, in: European Conference on Computational Fluid Dynamics, ECCOMAS CFD 2006, Egmond aan Zee, The Netherlands, 2006, pp. 5–8.

[37]. V. Bykov, A. Neagos, A. Klimenko, U. Maas, Hierarchical structure of slow manifolds of reacting flows, *Z. Phys. Chem*. 229 (2015) 833–856. DOI: 10.1515/zpch-2014-0599

[38]. R. Schießl, V. Bykov, U. Maas, et al., Implementing multi-directional molecular diffusion terms into Reaction Diffusion Manifolds (REDIMs), *Proc. Combust. Inst*. 36 (2017) 673–679. DOI: 10.1016/j.proci.2016.07.089

[39]. G. Stahl, J. Warnatz, Numerical investigation of time-dependent properties and extinction of strained methane and propane-air flamelets, *Combust. Flame* 85 (1991) 285–299. DOI: 10.1016/0010-2180(91)90134-W

[40]. J. Nafe, U. Maas, A general algorithm for improving ILDMs, *Combust. Theory Modelling* 6 (2002) 697–709. DOI: 10.1088/1364-7830/6/4/308

[41]. OpenFOAM: The Open Source CFD Toolbox [Online]. Available: https://www.openfoam.com. Accessed: 30 June 2020.

[42]. P.H. de Almeida Konzen, T. Richter, U. Riedel, U. Maas, Implementation of REDIM reduced chemistry to model an axisymmetric laminar diffusion methane–air flame, *Combust. Theory Model.* 15 (2011) 299–323. DOI: 10.1080/13647830.2010.538721

[43]. B. Merci, B. Naud, D. Roekaerts, U. Maas, Joint Scalar versus Joint Velocity-Scalar PDF Simulations of Bluff-Body Stabilized Flames with REDIM, *Flow Turbulence Combust*. 82 (2009) 185–209. DOI: 10.1007/s10494-008-9162-2

[44]. C. Strassacker, V. Bykov, U. Maas, Parametrization and projection strategies for manifold based reduced kinetic models, *Proc. Combust. Inst*. 37 (2019) 763–770. DOI: 10.1016/j.proci.2018.06.186

[45]. U. Prüfert, S. Hartl, F. Hunger, et al., A constrained control approach for the automated choice of an optimal progress variable for chemistry tabulation, *Flow Turbulence Combust.* 94 (2015) 593–617. DOI: 10.1007/s10494-015-9595-3

[46]. A.H.-D. Cheng, D.T. Cheng, Heritage and early history of the boundary element method, *Eng. Anal. Bound. Elem.* 29 (2005) 268–302. DOI: 10.1016/j.enganabound.2004.12.001

[47]. SanDiego-MEchanism, mechanical and Aerospace Engineering (Combustion Research), University of California at San Diego (2016).

[48]. R. Barlow, J. Frank, A. Karpetis, J.-Y. Chen, Piloted methane/air jet flames: Transport effects and aspects of scalar structure, *Combust. Flame* 143 (2005) 433–449. DOI: 10.1016/j.combustflame.2005.08.017

[49]. M. Bundy, A. Hamins, K. Y. Lee, Suppression limits of low strain rate non-premixed methane flames, *Combust. Flame* 133 (2003) 299–310. DOI: 10.1016/S0010-2180(03)00012-9

[50]. C.B. Oh, A. Hamins, M. Bundy, J. Park, The two-dimensional structure of low strain rate counterflow nonpremixed-methane flames in normal and microgravity, *Combust. Theory Model*. 12 (2008) 283–302. DOI: 10.1080/13647830701642201

[51]. G.P. Smith, D.M. Golden, M. Frenklach et al., "GRI-Mech 3.0," 1999. [Online]. Available: https://zbmath.org/software/7056?utm_source=.com [Accessed: Mar. 14, 2010].

[52]. H. Pitsch, H. Steiner, Large-eddy simulation of a turbulent piloted methane/air diffusion flame (Sandia flame D), *Phys. Fluids* 12 (2000) 2541–2554. DOI: 10.1063/1.1288493

[53]. H. Pitsch, Unsteady flamelet modeling of differential diffusion in turbulent jet diffusion flames, *Combust. Flame* 123 (2000) 358–374. DOI: 10.1063/1.1288493

[54]. A. Kronenburg, A. Papoutsakis, Conditional moment closure modeling of extinction and reignition in turbulent non-premixed flames, *Proc. Combust. Inst.* 30 (2005) 759–766. DOI: 10.1016/j.proci.2004.08.235

[55]. H. Chelliah, C.K. Law, T. Ueda, et al., An experimental and theoretical investigation of the dilution, pressure and flow-field effects on the extinction condition of methane-air-nitrogen diffusion flames, *Proc. Combust. Inst.* 23 (1991) 503–511. DOI: 10.1016/S0082-0784(06)80297-3

[56]. C. Yu, P. Breda, F. Minuzzi, et al., A novel model for incorporation of differential diffusion effects in PDF simulations of non-premixed turbulent flames based on reaction-diffusion manifolds (REDIM), *Phys. Fluids* 33 (2021) 025110. DOI: 10.1063/5.0039160

[57]. B.A.V. Bennett, M.D. Smooke, Local rectangular refinement with application to axisymmetric laminar flames, *Combust. Theory Model*. 2 (1998) 221–258. DOI: 10.1088/1364-7830/2/3/001

[58]. B.A.V. Bennett, Z. Cheng, R. Pitz, M.D. Smooke, Computational and experimental study of oxygen-enhanced axisymmetric laminar methane flames, *Combust. Theory Model*. 12 (2008) 497–527. DOI: 10.1080/13647830701843296